Aggregation and disaggregation processes in clusters of particles under flow: Simple numerical and theoretical insights

Louis-Vincent Bouthier [*] and Romain Castellani
Groupe CFL, CEMEF, Mines Paris, PSL Research University, 06904 Sophia Antipolis, France

Sébastien Manneville
ENSL, CNRS, Laboratoire de physique, F-69342 Lyon, France
and Institut Universitaire de France (IUF), 1 rue Descartes, 75231 Paris Cedex 05, France

Arnaud Poulesquen
CEA, DES, ISEC, DE2D, SEAD, LCBC, Université de Montpellier,
Marcoule, 30207 Bagnols-sur-Cèze Cedex Cedex, France

Rudy Valette and Elie Hachem
Groupe CFL, CEMEF, Mines Paris, PSL Research University, 06904 Sophia Antipolis, France

Aggregation and disaggregation of clusters of attractive particles under flow are studied from numerical and theoretical points of view. Two-dimensional molecular dynamics simulations of both Couette and Poiseuille flows highlight the growth of the average steady-state cluster size as a power law of the adhesion number, a dimensionless number that quantifies the ratio of attractive forces to shear stress. Such a power-law scaling results from the competition between aggregation and disaggregation processes, as already reported in the literature. Here we rationalize this behavior through a model based on an energy function, which minimization yields the power-law exponent in terms of the cluster fractal dimension, in good agreement with the present simulations and with previous works.

I. INTRODUCTION

Colloidal suspensions composed of attractive particles that aggregate into clusters when dispersed into a liquid medium have raised great interest for a number of decades due to their wide range of applications, from paints and coatings to food products or construction materials [1–8]. The large variety of attractive forces driving cluster aggregation, including van der Waals interactions, depletion or capillary forces, combined with stabilizing repulsive forces, such as electrostatic or steric interactions, lead to a complex phase diagram involving equilibrium liquid or phase-separated regimes as well as out-of-equilibrium gel or glassy phases [2,3,9,10]. Beyond their phase behavior at rest, understanding how colloidal suspensions respond to deformation and flow is pivotal for their processing and their practical use. Thus, a huge amount of work has been devoted to the rheology of colloidal suspensions and their structure under external mechanical solicitations [1–3,11,12]. In particular, one key question concerns the evolution of particle clusters under shear.

Colloidal clusters generically show a ramified structure characterized by a fractal dimension D linking the number of particles $n(l)$ in the cluster to its size l through $n(l) \propto l^D$ [13–15]. Other

---

*Corresponding author: louis.bouthier@etu.minesparis.psl.eu

structural parameters may be identified, such as the chemical dimension related to the number of bonds in the shortest path in a cluster [16], the connectivity, or the coordination number [17]. Since the seminal work of Weitz *et al.* [18,19] on diffusion-limited aggregation, a large number of experimental studies have characterized the microscopic mechanisms underpinning cluster formation at rest, either from direct visualization [20,21] or from scattering techniques [22]. In cases where colloidal aggregation leads to the formation of a space-spanning cluster network, i.e., to a colloidal gel, these measurements have provided key information on both the maximum cluster size ℓ and their fractal dimension D [23]. When shear is applied to a flocculated suspension, aggregates break up and form a suspension of isolated clusters. The steady-state cluster size distribution is a key observable and the dependence of ℓ and D on the shear stress applied to the suspension has been probed by combining light, x-ray, and neutron scattering and rheometry [24–27]. Typical results are that (i) ℓ decreases as a power law of the shear stress σ, $\ell \propto \sigma^{-m}$, with an exponent m ranging from 0.2 to 0.5 [28,29], and (ii) D increases from 1.8 to 2.2 depending on the specific aggregation mechanism to 2.4–2.7 under shear, a phenomenon known as "shear-induced cluster densification" [24,30].

Furthermore, thanks to the growth of computational capabilities over the past decade, large-scale numerical simulations have been developed to model suspensions, both at rest and under shear, with up to several millions of colloidal particles [31,32], sometimes taking into account the solvent through hydrodynamic interactions [33–37]. The model suspensions rely on various idealized two-body interaction potentials [38], which in some cases include bending stiffness [17,39,40] or solid friction [41–43]. One of the main advantages of numerical simulations is that they yield a complete picture of the cluster microstructure. Another modeling approach referred to as "population balance model" (PBM), relies on kinetic equations for "classes" of clusters of given sizes, which mimic the competition between aggregation and disaggregation processes through the use of various kernels [44–47]. Although some ingredients of the kernels can be theoretically predicted thanks to Smoluchowksi equations, in practice, PBM often require a significant amount of empirical tuning of the kernel parameters [15,48].

Strong theoretical predictions have also been derived from analytical models that relate microscopic parameters, such as the interparticle bond stiffness, to macroscopic quantities, such as the elastic modulus G' at rest, the yield strain γ_y, or the dynamic viscosity η under shear [12,49,50]. In particular, one popular model by Wessel and Ball [11] predicts that $\ell \propto \sigma^{-1/3}$ from a force balance under the assumption that the clusters behave hydrodynamically like compact spheres. While this model provides a correct estimate of the exponent m for various experiments [26], it does not account for the range of exponents reported in the literature [27,51,52], most probably due to the stringent assumption of hydrodynamically compact clusters. More refined models have considered soft, highly deformable clusters leading to $m = 1/2$ rather than $m = 1/3$ for rigid aggregates [53]. Yet, to the best of our knowledge, there is no general theoretical framework that may describe the behavior of colloidal clusters under an external stress.

The goal of the present paper is to propose very general theoretical arguments to predict the steady-state size ℓ of colloidal aggregates submitted to an external solicitation. Starting from dimensional analysis, we show in Sec. II that the competition between cluster aggregation and disaggregation can be captured through the minimization of an energy function. In Sec. III, we then provide evidence for the existence of an energy minimum in simple numerical simulations. We proceed to detail an analytical model in Sec. IV, which yields a power law for ℓ as a function of the adhesion number, a dimensionless number that quantifies the ratio of attractive forces to shear stress. Finally, this model is compared to the coagulation-fragmentation approach and to previous experimental and numerical findings in Sec. V. Conclusions and open questions are drawn in Sec. VI.

II. GENERAL FRAMEWORK

Before describing the general approach based on a grand-canonical free energy, we start with simple dimensional arguments to justify that the competition between cluster aggregation led by attractive forces and disaggregation driven by shear forces depends on a single dimensionless group, namely the adhesion number Ad, once the attraction range is fixed. As discussed in Refs. [41,54], attractive forces may be estimated by Ua/δ^2, with U the depth of the interaction potential between two particles, a the particle radius, and δ the range of interaction, which can be taken as the center-to-center distance between two particles at equilibrium or as the width of the potential well. Disaggregating forces, on the other hand, may be estimated by σa^2, with σ the external stress exerted on the clusters. One chooses here, as a distinction from the literature, to consider the stress rather than the shear rate because (i) whenever the shear rate is involved in similar definitions, it appears as multiplied by the solvent viscosity, therefore as a shear stress, and (ii) one is convinced that stress drives the disaggregation, like in plasticity or fracture [55–58], rather than a kinematic quantity. Following Ref. [54], the adhesion number is defined as the ratio of attractive forces to disaggregating forces:

$$\text{Ad} = \frac{U}{\sigma a \delta^2}. \tag{1}$$

The condition $\text{Ad} \ll 1$ implies that hydrodynamic forces dominate, while $\text{Ad} \gg 1$ indicates that attractive forces are predominant. It is important to note that the choice of this adhesion number contains some degree of arbitrariness. Indeed, other similar dimensionless groups may be built more generally by replacing $a\delta^2$ by $a^\alpha \delta^{3-\alpha}$, with $\alpha \in [0, 3]$, in Eq. (1). The precise choice depends on whether one considers energies ($\alpha = 0$), forces ($\alpha = 1$), or stiffnesses ($\alpha = 2$), i.e., energies per unit surface, or energies per unit volume ($\alpha = 3$). Finally, according to the Vaschy-Buckingham theorem [59–61], any characteristic length that depends on U, σ, a, and δ, such as the maximum cluster size ℓ, may be expressed as $\ell/a = \mathcal{F}(\text{Ad}, \delta/a)$. Therefore, a combination of both Ad and δ/a is expected. Also note that the adhesion number simply corresponds to the inverse of the "Mason number," $\text{Mn} = \sigma a^2 \delta/U$, a dimensionless group popular in the rheology community that quantifies the ratio of shearing forces to attractive forces [36,62,63].

In order to describe the competition between aggregation and disaggregation, we consider a grand-canonical ensemble with a population of clusters of mass $k \in \mathbb{N}^*$ associated to a number of clusters n_k. Each cluster of mass k has an associated energy $\mathcal{E}(k)$, which we seek to determine. The number of primary particles is not fixed and is related, for each cluster mass k, to a chemical potential α_k/β with $\beta = 1/(k_B T)$, with k_B as the Boltzmann constant and T the temperature. Note that the use of a canonical ensemble may seem more appropriate for a problem with a fixed number of particles. However, the calculation of the canonical partition function leads to the use of the complete Bell polynomials, where each variable is $e^{-\beta \mathcal{E}(k)}$. Inverting the relation is not straightforward, so that computing the distribution of clusters of mass k is very cumbersome within a canonical framework. Here, thanks to the grand-canonical formulation, $\mathcal{E}(k)$, as well as the energy $n_k \mathcal{E}(k)$ associated to all clusters of mass k, may be computed rather easily. The grand-canonical partition function reads:

$$\Xi = \sum_{(n_k)_{k \in \mathbb{N}^*} \in \mathbb{N}^{\mathbb{N}^*}} \exp\left[-\sum_{k \in \mathbb{N}^*} (\beta n_k \mathcal{E}(k) - n_k k \alpha_k) \right], \tag{2}$$

$$= \prod_{k \in \mathbb{N}^*} [1 - e^{-\beta \mathcal{E}(k) + k\alpha_k}]^{-1}. \tag{3}$$

The convergence of the series in Eq. (2) is guaranteed if $\alpha_k k < \beta \mathcal{E}(k)$ for all $k \in \mathbb{N}^*$. Moreover, it follows from Eq. (2) that the distribution of each level population n_k is a geometric distribution with a parameter $e^{-\beta \mathcal{E}(k) + k\alpha_k}$. Since the average number of particles $\langle N \rangle$ is related to the average population $(\langle n_k \rangle)_{k \in \mathbb{N}^*}$ of clusters of mass k through $\langle N \rangle = \sum_{k \in \mathbb{N}^*} k \langle n_k \rangle$, one may compute the

average number of clusters of mass k and the standard deviation through:

$$\langle n_k \rangle = -\frac{1}{k} \frac{\partial \ln \Xi}{\partial \alpha_k} = [e^{\beta \mathcal{E}(k) - \alpha_k k} - 1]^{-1}, \tag{4}$$

$$\Delta n_k = \frac{1}{k} \sqrt{\frac{\partial^2 \ln \Xi}{\partial \alpha_k^2}} = \sqrt{\langle n_k \rangle (1 + \langle n_k \rangle)} = \frac{1}{2} \operatorname{csch} \left[\frac{\beta \mathcal{E}(k) - \alpha_k k}{2} \right], \tag{5}$$

which boils down to the Bose-Einstein statistics.

In practice, in an experiment or a simulation, a initial sample of $(n_k)_{k \in \mathbb{N}^*}$ is chosen, which evolves in time according to external conditions. It is clear from the above expressions that the $(n_k)_{k \in \mathbb{N}^*}$ should end up being centered around the averages $(\langle n_k \rangle)_{k \in \mathbb{N}^*}$ with a dispersion $(\Delta n_k)_{k \in \mathbb{N}^*}$. Therefore, a higher number of clusters of mass k also brings a higher dispersion around this value. Since numerical simulations yield a probability distribution function $f(k)$ for the number of cluster of mass k, which is assumed to be equal to the average distribution $\langle n_k \rangle$, i.e., $f(k) = \langle n_k \rangle$, one can find the average potential energy of the clusters and the standard deviation respectively through:

$$\beta \mathcal{E}(k) - \alpha_k k = \ln \left[1 + \frac{1}{f(k)} \right], \tag{6}$$

$$\Delta(\beta \mathcal{E}(k) - \alpha_k k) = \{f(k)[1 + f(k)]\}^{-\frac{1}{2}} = 2 \sinh \left[\frac{\beta \mathcal{E}(k) - \alpha_k k}{2} \right], \tag{7}$$

$$> \beta \mathcal{E}(k) - \alpha_k k. \tag{8}$$

III. NUMERICAL SIMULATION

A. Numerical scheme and analysis

To get some insight of the competition between aggregation and disaggregation processes, we turn to simple molecular dynamics simulations of two-dimensional Couette and Poiseuille flows based on the LAMMPS library [64]. We use reduced units, where the unit size is given by the particle radius. The simulation box is of size $\mathcal{L} \times h$ with periodic boundary conditions along the x direction and solid boundaries along the y direction located at $y = 0$ and $y = h$. The length of the box $\mathcal{L}$ is fixed to $\mathcal{L} = 620$, and the width h is either 103 or 206, much larger than the particle size. Each boundary is constituted of one layer of particles of unit size which positions are fixed and that interact with bulk particles through a repulsive Yukawa potential $w_s(r) = 100e^{-r}/r$, with r the distance between two particles and a cut-off distance $r = 5$ to save computation time. This choice of a purely repulsive potential leads to some depletion of the particles at the walls but allows us to avoid irreversible aggregation on the walls and to focus on bulk aggregation-disaggregation processes. Finally, the interaction potential between two particles in the bulk is a classical 12-6 Lennard-Jones potential $w(r) = 4(r^{-12} - r^{-6})$ with a cut-off distance $r = 40$, again to save computation time.

First, the system is initialized with a particle surface fraction of $\phi = 0.12$. Using a canonical formulation, the temperature is fixed at $T = 0.01$. The time step is taken as $\Delta t = 0.01$, which is small enough to account realistically for temporal variations while keeping the computation time reasonably low. Particles are distributed over a square lattice, and their initial velocities are chosen according to a Maxwell distribution for the given temperature. The system is then let to evolve for a duration 5000 time units in order to create the initial cluster distribution. More precisely, the equation of motion for each particle $i \in [\![1, N]\!]$, with N the total number of particle, is

$$\frac{d^2 \boldsymbol{r}_i}{dt^2} = -\frac{\partial \mathcal{W}}{\partial \boldsymbol{r}_i} [(\boldsymbol{r}_j)_{j \in [\![1,N]\!]}] + \boldsymbol{B}_i, \tag{9}$$

$$\mathcal{W}[(\boldsymbol{r}_j)_{j \in [\![1,N]\!]}] = \sum_{k=1}^{N} \sum_{j=k+1}^{N} w(|\boldsymbol{r}_k - \boldsymbol{r}_j|), \tag{10}$$

$$w(r) = 4(r^{-12} - r^{-6}), \tag{11}$$

with $\boldsymbol{r}_i$ the position of particle i and $\boldsymbol{B}_i$ a Brownian white noise for particle i.

In a second step, a drag force $\boldsymbol{F}_i = C(\boldsymbol{u} - \frac{d\boldsymbol{r}_i}{dt})$ is applied on each particle $i \in [\![1, N]\!]$, with $C = 1$ the drag coefficient [66] and $\boldsymbol{u} = Vy/h\boldsymbol{e}_x$ for the 2D Couette flow or $\boldsymbol{u} = 4V(1 - y/h)y/h\boldsymbol{e}_x$ for the 2D Poiseuille flow, where V is the maximum flow velocity. Here a microcanonical formulation is used and the time step is set to $\Delta t = 0.001$. The simulation is run for a duration of 1000 time units. The equation of motion for each particle i thus reads:

$$\frac{d^2\boldsymbol{r}_i}{dt^2} = -\frac{\partial \mathcal{W}}{\partial \boldsymbol{r}_i}[(\boldsymbol{r}_j)_{j\in[\![1,N]\!]}] + F(\boldsymbol{r}_i)\boldsymbol{e}_x, \tag{12}$$

$$F(\boldsymbol{r}_i) = C\left[-\frac{d\boldsymbol{r}_i}{dt} \cdot \boldsymbol{e}_x + V\frac{\boldsymbol{r}_i \cdot \boldsymbol{e}_y}{h}\begin{cases}1 & \text{2D Couette flow} \\ 4\left(1 - \frac{r_i \cdot e_y}{h}\right) & \text{2D Poiseuille flow}\end{cases}\right]. \tag{13}$$

The parameters investigated in the present work are $(V, h) \in \{0.1, 0.3, 1, 3, 10, 30, 100\} \times \{103, 206\}$. The values of the adhesion number are then $\text{Ad} \in \{1, 2, 3, 6, 10, 20, 34, 68, 103, 206, 344, 688, 1032, 2065\}$. The numerical scheme used here is a velocity Verlet algorithm [67]. The computations output are (i) the position of the particles at each time step and (ii) the clusters to which the particles belong based on a connected-component algorithm [68] with a distance threshold of 1.4, consistently with the literature [39,69,70]. Moreover, we checked that for thresholds ranging from 1.1 to 2.0, the distribution of neighbors does not change, so that the results are not sensitive to the specific choice of threshold. The size of cluster number I is quantified according to the following estimates:

(i) the radius of gyration R_g^I given by

$$R_g^I = \sqrt{\frac{1}{|P(I)|} \sum_{k \in P(I)} \|\boldsymbol{r}_k - \bar{\boldsymbol{r}}\|^2}, \tag{14}$$

$$\bar{\boldsymbol{r}} = \frac{1}{|P(I)|} \sum_{k \in P(I)} \boldsymbol{r}_k, \tag{15}$$

with $\boldsymbol{r}_k$ the position of the particles in the cluster, $P(I)$ the set of particles in cluster I and $|P(I)|$ the number of particles in cluster I.

(ii) the Feret radii in the x and y directions given by $[\max_{k \in P(I)} \boldsymbol{r}_k \cdot \boldsymbol{e}]/2 - [\min_{k \in P(I)} \boldsymbol{r}_k \cdot \boldsymbol{e}]/2$ with $\boldsymbol{e}$ the unit vector in the x and y directions, respectively.

(iii) the half maximum chord length given by $\max_{(k,l) \in P(I)^2} \|\boldsymbol{r}_k - \boldsymbol{r}_l\|/2$.

In order to infer statistical estimations, each size distribution is further weighted by the number of particles in each cluster. Such weighting is needed because the number of clusters is not constant. Therefore, because the total number of particles is constant, weighting by the mass of each cluster allows one to recover the number of particles when integrating over the whole distribution. Finally, thanks to the reduced units, $U/a\delta^2 = 1$ and the shear stress is $\sigma = CV/h = V/h$ here due to $C = 1$ so that the adhesion number simply reads $\text{Ad} = h/V$. Note that, due to the specific choice of interaction potentials and to the absence of thermal motion and hydrodynamic interactions, the present simulations remain very crude. Thus, their aim is rather to offer a generic view of the evolution of particulate clusters under flow that supports our theoretical approach, than to provide a detailed, realistic picture of the interplay between flow and colloidal interactions at the particle scale.

B. Simulation results

Figure 1 shows typical particle distributions computed after the preparation step prior to shearing [Fig. 1(a)], and after application of shear in the Couette geometry [Fig. 1(b)], in spite of some depletion at the walls. It appears clearly that the system starts from a space-spanning ramified structure and evolves toward dense, isolated clusters under shear. Moreover, as shown in Fig. 1(c), the different estimates for the cluster size yield consistent values. In the following, for the sake of
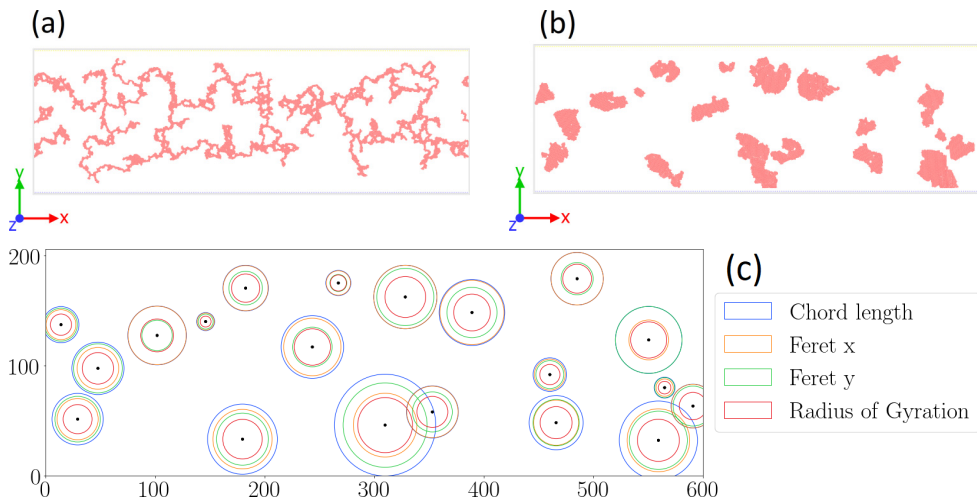
FIG. 1. Simulated particle distributions for $V = 10$, $h = 206$, and $C = 1$ after the preparation step prior to shearing (a) and at after shearing in the Couette geometry (b). Rendering using Ovito [65]. (c) Cluster detection and various estimates of the cluster size as defined in the text for the top right particle distribution.

simplicity, we shall focus only on the weighted average of the radius of gyration to estimate the cluster size ℓ.

Following the general framework introduced in Sec. II, we compute the distribution of the cluster mass and the dimensionless energy $\beta\mathcal{E}(k) - \alpha_k k$ based on Eq. (6). Figure 2 shows this energy functional plotted against the mass k of particles within a cluster for adhesion numbers ranging from 1 to about 2000. More specifically, from our simulations, we extract a probability density function of the steady-state cluster population in terms of sizes. This probability density function is directly imported into Eq. (6) as $f(k)$, which yields the dimensionless energy $\beta\mathcal{E}(k) - \alpha_k k$. Focusing on one particular curve, when the probability density function goes to 0, the dimensionless energy goes to infinity, which shows that these states are impossible to access. Also, when the probability density function is maximum, the dimensionless energy is minimum because the most probable
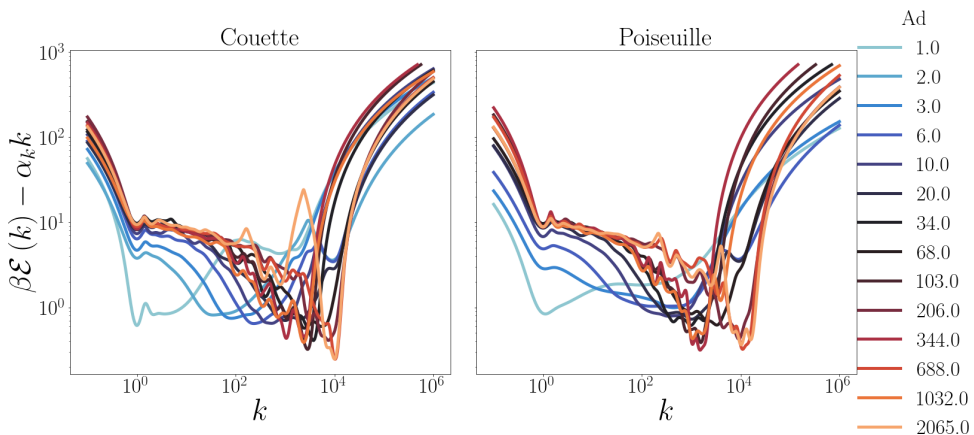

FIG. 2. Energy functional $\beta\mathcal{E}(k) - \alpha_k k$ computed from from Eq. (6) as a function of the number k of particles in a cluster for (left) Couette flow and (right) Poiseuille flow. Colors correspond to the adhesion number Ad as indicated in the legend. Results obtained from simulations performed with $h = 103$ or $h = 206$.
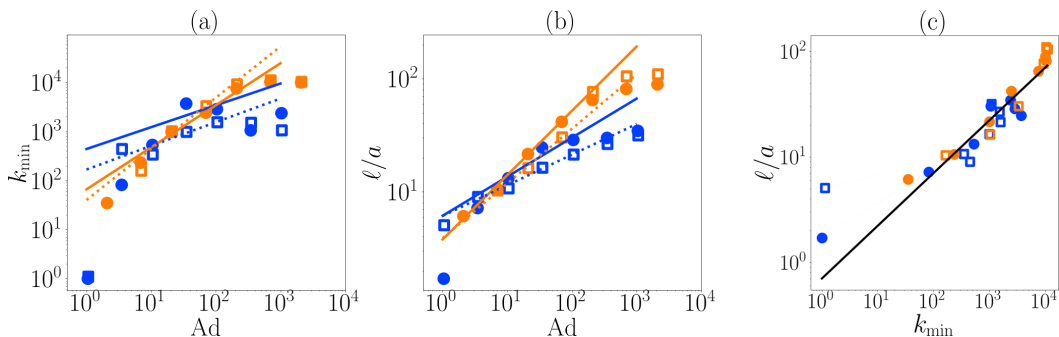
FIG. 3. (a) Mass $k_{\min}$ of the clusters corresponding to the energy minimum and (b) cluster size ℓ defined as the weighted average of the radius of gyration of the clusters, as a function of the adhesion number Ad for Couette flow (●) and Poiseuille flow (□) and for two different width $h = 103$ (blue) and $h = 206$ (orange). Solid and dotted lines correspond to the best power-law fits respectively for the Couette and the Poiseuille flow, and computed over Ad $\in [2, 200]$. (c) Cluster size ℓ as a function of the equilibrium mass $k_{\min}$. The black solid line corresponds to $\ell \propto k_{\min}^{1/2}$. Same symbols and colors as in (a) and (b).

size minimises the global energy functional. Looking at the small- and large-mass limits, it appears that $\lim_{k \to 0^+} \beta \mathcal{E}(k) - \alpha_k k = \lim_{k \to +\infty} \beta \mathcal{E}(k) - \alpha_k k = +\infty$, which indicates that extreme masses are not accessible to the system. Second, in all cases, there exists a global minimum of the energy functional that shifts toward larger values of k as the adhesion number Ad is increased. As expected intuitively, this suggests that the average cluster mass increases with Ad. Moreover, the steeper slope $\partial_k[\beta \mathcal{E}(k) - \alpha_k k]$ of the energy functional on the right side of the global minimum than on the left side indicates that the system reaches the energy minimum more rapidly when starting from large masses than from small masses. This confirms the intuition that disaggregation processes are much faster than aggregation processes. Third, while the value of the global minimum energy does not show any clear trend with Ad, there may exist several local minima in $\beta \mathcal{E}(k) - \alpha_k k$. This means that several metastable states may occur. These states may disappear when increasing the simulation duration or the system size. Still, this shows that a rather polydisperse population of clusters may be found, at least transiently. This may also be related to the dispersion in the energy minimum illustrated previously.

Figures 3(a) and 3(b) respectively show the "equilibrium mass" $k_{\min}$ of the clusters corresponding to the energy minimum, i.e., $k_{\min} = \arg\min_{k \in \mathbb{R}_+}[\beta \mathcal{E}(k) - \alpha_k k]$, and the cluster size ℓ/a taken as the weighted average of their radius of gyration plotted against the adhesion number Ad. For both observables, a power-law regime is identified over almost two decades in adhesion numbers. The exponents inferred from power-law fits for Ad $\in [2, 200]$ are reported in Table I. For Ad $\gtrsim 100$, a saturation is observed in $k_{\min}$ together with large variations, for both the Couette and Poiseuille flows. This behavior is most probably linked to finite-size effects as the average cluster size becomes comparable or larger than the system width h. Consistently with Fig. 3(a), the cluster size ℓ increases as a power law of Ad [Fig. 3(b)]. There, although the data for ℓ do not show such a strong saturation as for $k_{\min}$, significant deviations from power-law behavior are still observed for Ad $\gtrsim 100$.

Moreover, the exponents for the dependence of ℓ with Ad seem to depend significantly on the geometry, with values 0.35 and 0.57 for the Couette flow and 0.27 and 0.48 for the Poiseuille flow, respectively for $h = 103$ and $h = 206$ (see Table I). Similarly, the corresponding exponents for $k_{\min}$, namely 0.4 and 0.9 for Couette flow and 0.5 and 1.0 for Poiseuille flow, also differ for the two values of h. At this stage, the reason for such an influence of h in the simple two-dimensional simulations remains unclear, and future work should focus on more realistic interaction potentials and three-dimensional geometries.

Still, it is interesting to note that ℓ/a and $k_{\min}$ are not expected to have the same power-law behavior with the adhesion number because of their intrinsic relationship. More specifically,

TABLE I. Exponents and prefactors of the power-law fits in Fig. 3 for the different geometries, widths, and sizes ℓ and $k_{\min}$.

Geometry	h	Variable	Exponent	Prefactor
Couette	103	ℓ/a	0.346 ± 0.009	6.1 ± 0.2
Couette	103	$k_{\min}$	0.4 ± 0.4	400 ± 700
Couette	206	ℓ/a	0.57 ± 0.03	3.5 ± 0.4
Couette	206	$k_{\min}$	0.9 ± 0.1	60 ± 30
Poiseuille	103	ℓ/a	0.271 ± 0.007	6.1 ± 0.2
Poiseuille	103	$k_{\min}$	0.5 ± 0.1	170 ± 70
Poiseuille	206	ℓ/a	0.48 ± 0.03	3.9 ± 0.5
Poiseuille	206	$k_{\min}$	1.0 ± 0.1	40 ± 20

considering the framework of fractal clusters, the number of particles in a cluster k is related to the geometrical size l through $k = (l/a)^D$ with D the fractal dimension. In the two-dimensional case, D should fall into the range [1, 2]. Figure 3(c) shows that $\ell/a \propto k_{\min}^{1/2}$, which is compatible with a fractal dimension $D \simeq 2$, i.e., with almost dense aggregates in two dimensions geometries. The fact that very compact aggregates are obtained in the simulations is confirmed visually by looking at Fig. 1(b). Another confirmation comes from the ratio of the exponent for $k_{\min}$ and that for ℓ/a in Table I, which is also found to be close to 2 (except for the Couette flow with $h = 103$ but the scatter of the $k_{\min}$ data in this latter case makes it difficult to conclude).

IV. PROPOSITION OF MODEL

A. Description of the disaggregation and reaggregation processes

The precise internal structure of the aggregates is really complex and depends on many different parameters including the volume fraction, the nature of the interparticle forces and of the solvent, temperature, and chemical environment. Hence, we shall consider the aggregates as a continuum without further internal details. We consider a suspension of particles of size a that interact through an attractive potential so that they gather into aggregates as sketched in Fig. 4. Following a statistical approach as in Refs. [48,71–74], we assume that there exists a distribution $f(t, l, a, U, \delta, \sigma)$ giving the population of aggregates of size l at time t made of particles of size a interacting through
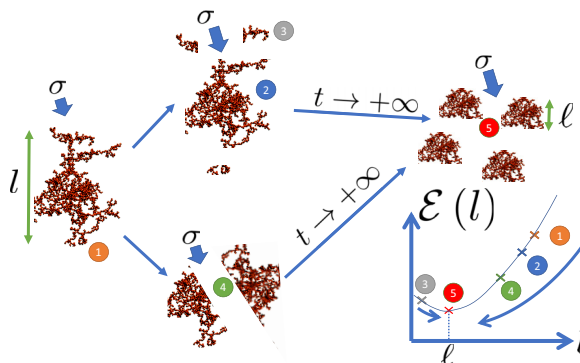

FIG. 4. Sketch of the disaggregation and reaggregation processes under a uniform external stress σ. The numbers represent different sizes of aggregates with different levels of energy. The aggregates are disaggregating and reaggregating according to the stress solicitation. Transition from state 1 to states 2 and 4 corresponds to a "fragile" rupture, while transition from state 1 to state 3 is an "erosion" process.

a pair potential U over a distance δ under a stress solicitation σ. Such a distribution may be computed through a coagulation-fragmentation equation as in Refs. [48,71,74]. Yet, this approach requires to identify coagulation kernels and fragmentation coefficients, which involves much effort for theoretical and/or numerical validation. Without ignoring the power of such tools, we aim at a simpler approach through the present statistical approach.

We start by imposing the conservation of the total number of particles N, which reads:

$$N = \int_0^{+\infty} n\left(\frac{l}{a}\right) f(t, l, a, U, \delta, \sigma)\, dl = \text{const}, \tag{16}$$

where $n(l/a)$ denotes the number of particles per cluster of relative size l/a. The average size of the aggregates is thus given by:

$$\bar{l}(t, a, U, \delta, \sigma) = \frac{a}{N} \int_0^{+\infty} n\left(\frac{l}{a}\right) \frac{l}{a} f(t, l, a, U, \delta, \sigma)\, dl. \tag{17}$$

From a statistical point of view, and assuming that the aggregates are submitted to a uniform external stress σ far from any boundary, aggregates should evolve from one state to another as sketched in Fig. 4. If the stress is sufficiently large to break some initial aggregate (state 1), then a disaggregation occurs either due to "fragile" rupture into two pieces of similar sizes (bottom part of Fig. 4, state 4) or due to "erosion," where small pieces detach from the initial aggregate (top part of Fig. 4, states 2 and 3). If the larger pieces can still be broken down (states 2 and 4), then the process continues. However, if the pieces become too small (state 3), then the interparticle attraction dominates and reaggregation occurs. In the process, the aggregates progressively decrease their global energy, until a minimum is reached at long times $t \to +\infty$. Therefore, the steady state (state 5) eventually corresponds to the optimum of all possible sizes, which results from a dynamical equilibrium between disaggregation and reaggregation processes. More formally, when a steady state is reached, the average aggregate size ℓ is given by

$$\ell(a, U, \delta, \sigma) = \lim_{t \to +\infty} \bar{l}(t, a, U, \delta, \sigma). \tag{18}$$

In practice, since t remains finite, we note that the longer the final time, the smaller the spread of the distribution around the steady-state size. An additional comment is that, keeping the previous set of variables for the distribution f, an equivalent form using the Vaschy-Buckingham theorem [59–61] is found by replacing $f(t, l, a, U, \delta, \sigma)dl$ with $\tilde{f}(l/a, \text{Ad}, \delta/a)d(l/a)$, where t can be discarded based on unit independence. Time becomes relevant, however, when the viscosity η of the suspending liquid or any other time-related quantity is considered.

B. Analytical formulation of the model

Let us consider a suspension of particles of diameter a gathered in aggregates. The bond between each particle involves an energy U and an interparticle distance of separation δ. The system is submitted to a uniform stress σ. One aims at estimating the steady-state size of stable aggregates ℓ as a function of a, U, δ, and σ. Following Eggersdorfer *et al.* [42], for a dense aggregate of size l, the applied mechanical energy per unit area is σl. However, aggregates are not completely dense and one should more generally account for their fractal nature. As already introduced above in Sec. III B, the number of particles in an aggregate of size l is proportional to $(l/a)^D$ with D the fractal dimension of the clusters. Each particle in the aggregates contributes to the overall energy per unit surface. As if they were in parallel, the mechanical energy per unit surface should be weighted by the number of particles in an aggregate because there is fluid flowing inside the aggregates, which interferes with each particle. Hence, on the one hand, the mechanical energy per unit of effective surface of the aggregate $M(l)$ is proportional to $\sigma a(l/a)^{D+1}$. On the other hand, if one isolates an aggregate of size l, then the energy per unit surface liberated due to broken bonds E is $E(l) = U\delta^{-2}$, which is independent of the size l [54]. Indeed, considering an intermolecular potential $w(d)$, with

d the intermolecular distance, one can compute the interparticle potential per unit area through:

$$W(d) = 2\pi \varrho^2 \int_d^{+\infty} \int_y^{+\infty} \int_0^{+\infty} r w(\sqrt{r^2 + z^2}) \, dr dz dy, \tag{19}$$

where ϱ is the molecular density inside a particle. Defining δ as the distance that satisfies $W'(\delta) = 0$, or equivalently $\delta = \arg \min_{d \in \mathbb{R}_+^*} W(d)$ [75], and the energy $U = \delta^2 W(\delta)$, $E(l) = U\delta^{-2}$ indeed corresponds to the energy per unit surface liberated due to broken bonds. This energy is independent of the size of the aggregate because one may assume that, on the boundary of the aggregate, the number of particles per unit surface does not depend on l and is only related to the structure, which is assumed to be fixed in steady state. Finally, the steady-state size ℓ corresponds to the size for which the mechanical energy balances that due to broken bonds, i.e., $M(\ell) = E(\ell)$, which leads to:

$$\frac{\ell}{a} = \left(\frac{U}{\sigma a \delta^2} \right)^{\frac{1}{1+D}} = \mathrm{Ad}^{\frac{1}{1+D}}. \tag{20}$$

The same result can be obtained by minimizing the total energy $\mathcal{E}(l) = l^2[M(l) - E(l)]$. Another way to consider this concept is to relate it to Eggersdorfer *et al.* [42]. Indeed, on the one hand, if a stress σ is applied on a cluster of size l with $(l/a)^D$ particles of size a, then one may assume that the stress is shared in parallel on all particles, which gives a force $F_{\min} = \sigma a^2$. On the other hand, if the stress is focused on one single particle, then there is a force $F_{\max} = \sigma l^2$. Taking the geometrical average of these two extremes leads to $F_{\mathrm{avg}} = \sqrt{F_{\min}F_{\max}} = \sigma l a$. This average force should be summed over the whole chain with $(l/a)^D$ elements, which reads $F_{\mathrm{tot}} = \sigma l a (l/a)^D = \sigma a^2 (l/a)^{1+D}$. Finally, the bearable force between two particles is Ua/δ^2. Therefore, the link breaks when $\sigma a^2 (\ell/a)^{1+D} = Ua/\delta^2$, leading to $\ell/a = \mathrm{Ad}^{\frac{1}{1+D}}$ as in Eq. (20). Equation (20) also agrees with Eq. (18) through the Vaschy-Buckingham theorem [59–61]. Indeed, Eq. (18) may be rewritten as:

$$\frac{\ell}{a} = G\left(\mathrm{Ad}, \frac{\delta}{a} \right). \tag{21}$$

Adding that U/δ^2 provides all the information about the interaction potential, one has $\partial_{\delta/a}G = 0$ and thus

$$\frac{\ell}{a} = G(\mathrm{Ad}), \tag{22}$$

consistently with Eq. (20). Note that this model may show some limitations especially in the case of very loose aggregates, e.g., fibers or linear chains of adhesive spheres of length l, for which the hydrodynamic stress grows as l^3 due to the transmission of stresses by lubrication forces. This would bring an evolution of the hydrodynamic energy as l^5, or of the hydrodynamic force as l^4, which are, to our knowledge, not reported in the literature.

V. DISCUSSION

In this section, we discuss the theoretical approach and numerical results in light of the literature. We start by comparing the model with the classical coagulation-fragmentation approach. Then, the power-law scaling predicted for the cluster size, $\ell \propto \mathrm{Ad}^{1/(1+D)}$, is confronted to the present simulations and to previous experimental results.

A. Comparison with a coagulation-fragmentation model

The model proposed above in Sec. IV may be compared to the coagulation-fragmentation approach introduced in the literature in the late 1980s [76] and subsequently enriched over the years, e.g., through the population balance models [46–48,71]. In such an approach, the probability

density function f of clusters of size x at time t obeys the following dynamical equation:

$$\frac{\partial f}{\partial t}(t, x, \bullet) = \frac{1}{2} \int_0^x K(y, x - y, \bullet) f(t, y, \bullet) f(t, x - y, \bullet) \, dy$$

$$- \frac{1}{2} \int_0^x F(y, x - y, \bullet) f(t, x, \bullet) \, dy - \int_0^{+\infty} K(x, y, \bullet) f(t, x, \bullet) f(t, y, \bullet) \, dy$$

$$+ \int_0^{+\infty} F(x, y, \bullet) f(t, x + y, \bullet) \, dy, \tag{23}$$

with $\bullet = (a, U, \delta, \sigma)$, K the aggregation kernel and F the fragmentation kernel. Considering the long-term behavior, it can be shown that f takes the general form [48,71,76]:

$$f(t, x, \bullet) = \frac{1}{s^2(t, \bullet)} \varphi \left[\frac{x}{s(t, \bullet)}, \bullet \right], \tag{24}$$

where s and φ are two functions that depend only on time and size, respectively, and such that $\int_{\mathbb{R}_+} x \varphi(x, \bullet) \, dx = N$, the fixed total number of particles. The function s corresponds to the average mass of the clusters according to the distribution f. It can be related to a size through the cluster fractal dimension D by $s \propto l^D$. Then, integrating the previous expression over the size as in Eq. (17), one computes the steady-state average size as:

$$\bar{l}(t, \bullet) = a s^{\frac{1}{D}}(t, \bullet), \tag{25}$$

with

$$\lim_{t \to +\infty} s(t, \bullet) = \left[N \frac{A(\bullet)}{B(\bullet)} \right]^{\frac{1}{\alpha + 2 - \lambda}}, \tag{26}$$

$$A(\bullet) = \iint_{\mathbb{R}_+^2} x y \varphi(x, \bullet) \varphi(y, \bullet) K(x, y, \bullet) \, dx dy, \tag{27}$$

$$B(\bullet) = \iint_{\mathbb{R}_+^2} x y \varphi(x + y, \bullet) F(x, y, \bullet) \, dx dy, \tag{28}$$

where λ and α are the respective homogeneity coefficients of K and F [77], assuming $\alpha + 2 > \lambda$. It follows from Eqs. (18), (25), and (26) that

$$\frac{\ell}{a} = \left[N \frac{A(\bullet)}{B(\bullet)} \right]^{\frac{1}{D(\alpha + 2 - \lambda)}}. \tag{29}$$

Finally, identifying with Eq. (20), one gets

$$\frac{U}{\sigma a \delta^2} = \left[N \frac{A(\bullet)}{B(\bullet)} \right]^{\frac{1+D}{D(\alpha + 2 - \lambda)}}. \tag{30}$$

Most of the physical quantities appear as multiplicative factors, in the sense that, for example, the coagulation kernel K is usually built with a factor U/η with η the viscosity of the fluid and no other dependence on physical quantities besides the variables x and y. Therefore, the ratio $NA(\bullet)/B(\bullet)$ can be considered as the product of a dimensionless number built in a similar manner as the adhesion number and another factor that depends only on the shape of respective kernels without involving any additional physical parameter. Therefore, in order to keep Eq. (30) true in general, one should impose that the exponent is 1, which leads to

$$1 = D(\alpha + 1 - \lambda). \tag{31}$$

This is an important result which, to our knowledge, has not been reported in the literature before. Indeed, Eq. (31) allows one to relate the first mechanical approach to population balance
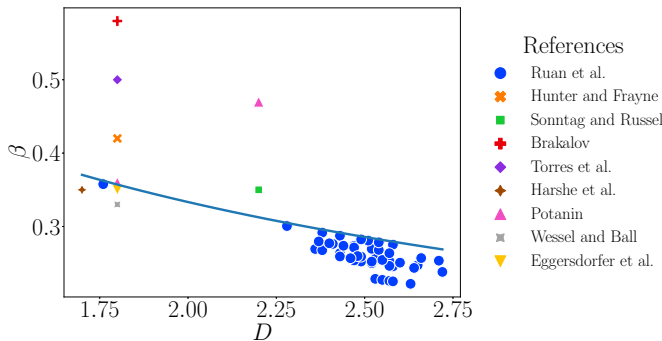
FIG. 5. Power-law exponent β in $\ell/a = \mathrm{Ad}^\beta$ as a function of the fractal dimension D of the aggregates extracted from Refs. [11,26–29,41–43,51,52,84–90] (●) and compared to the model prediction $\beta = (1 + D)^{-1}$ (solid line).

models, where the homogeneity coefficients may seem disconnected from physical and measurable quantities. This result also emphasizes the fact that the adhesion number is a correct measure of the relative importance of aggregation versus disaggregation.

We note that aggregation kernels are pretty well covered, either in terms of theoretical solutions [48,71,78,79] with simple sums or products or in terms of a physical construction, e.g., based on collisions, thermal fluctuations, and diffusion [80,81]. Fragmentation kernels, however, are more poorly controlled, in the sense that some theoretical solutions impose some strong conditions on these kernels without much physical justification [46–48,71], so that the expressions of the fragmentation kernels remain mostly empirical or semiempirical [82,83]. Therefore, although the use of coagulation-fragmentation equations is well established, relating some of the main terms to physical phenomena, such as the interaction potential and the flow stresses, is an important step yet to be fully achieved.

B. Comparison with simulations and experiments

Relating the model proposed in Sec. IV to the simulations of Sec. III, we expect the exponents in Table I to be linked to the fractal dimension respectively by $1/(1 + D)$ for the steady-state size ℓ, and $D/(1 + D)$ for the equilibrium mass $k_{\min}$. The broad variability of the exponents does not allow us to properly extract a fractal dimension from the simulations. Nevertheless, as discussed above in Sec. III B, the shear-induced clusters are almost dense, so that we may assume a fractal dimension D close to 2. Such a compactness most probably results from the specific interaction potential, i.e., a 12-6 Lennard-Jones potential, which is a central-force potential and is likely to lead to clusters with dropletlike shapes. We note that $D = 2$ would be consistent with the exponent $\beta = (1 + D)^{-1} = 1/3$ expected for ℓ as a function of Ad, at least in the smaller geometry, since Table I reports exponents of 0.35 and 0.27 for $h = 103$.

Moreover, the results may be compared to the recent three-dimensional simulations under simple shear flow by Ruan *et al.* [43], which also report rather dense shear-induced clusters at steady state. Focusing both on the cluster size and on the average number of particles in a cluster as in the present work, the authors extract the cluster fractal dimension D and show that ℓ/a scales as a power law of the shear stress. The exponents β for ℓ reported in Ref. [43] are replotted as a function of D as blue circles in Fig. 5 and show good agreement with the prediction $\beta = (1 + D)^{-1}$. Note that this is also consistent with the empirical expression proposed in Ref. [43], namely $\beta = S/(S + \langle D \rangle)$, where $\langle D \rangle$ denotes the average cluster fractal dimension, and the fitting parameter S is found to be close to 1.

TABLE II. Experimental parameters and measurements of the aggregate size from the literature. ℓ_{exp} is the direct measurement of the aggregate size, while ℓ_{th} is the aggregate size estimated using Eq. (20) based on the parameters defined in the text and reported in the references of the first column.

Source	[36,91–93]	[21,94–96]
ℓ_{exp} (nm)	500	60
a (nm)	150	6.5
$U/k_B T$	20	60
σ (MPa)	0.1	2
δ (Å)	7	2
D	2.6	1.88
ℓ_{th} (nm)	300	55

On the experimental side, a number of works have reported results assessing the size of aggregates under the application of a mechanical stress. However, only a handful of papers explicitly state the values of the various parameters a, U, σ, δ, and D. Table II and Fig. 5 gather a selection of such previous works. First, Table II shows that Eq. (20) predicts a typical cluster size ℓ_{th} which is of the same order as the experimental size ℓ_{exp}. All the parameters fall into commonly known ranges and justify that the previous approach may be a good proxy to evaluate the most stable cluster size. Second, Fig. 5 probes the sensitivity of ℓ/a with the adhesion number Ad by plotting the power-law exponent β in $\ell/a = \text{Ad}^\beta$ as a function of D. Except for a few points that lie far from the average estimation, most exponents are gathered along the prediction of Eq. (20), consistently with the numerical results of Ref. [43], which provides strong support for the approach described in Sec. IV.

Finally, Fig. 6 provides a sensitivity study of the value of ℓ on the different parameters of Eq. (20) based on Table II. It is clear that the most critical parameters are D and δ as expected from Eq. (20). Therefore, particular attention must be considered to assess accurately these parameters. Yet when one of these two parameters are unknown, the model can be used to estimate D or δ with good accuracy based on measurements of ℓ.

VI. CONCLUSION

We have investigated simple two-dimensional numerical simulations and proposed a theoretical description of aggregation and disaggregation processes in colloidal dispersions under shear. We have shown that the classically reported power-law increase of the average cluster size with the
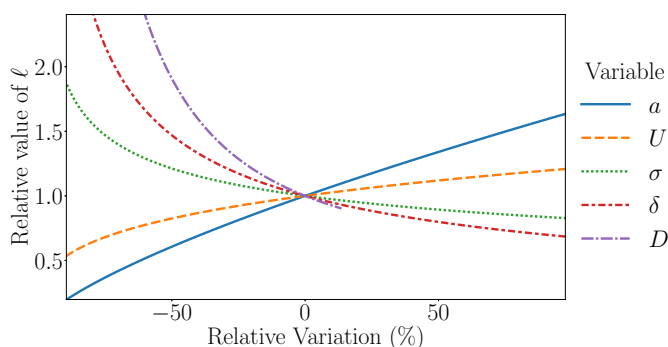

FIG. 6. Sensitivity study of ℓ predicted by Eq. (20) on relative variations of the different control parameters around the values listed in the first line of Table II except for the fractal dimension, which is varied from 1 to 3.

adhesion number can be rationalized through a dynamical balance of energy between aggregation and disaggregation. More precisely, a statistical physics approach allowed us to make a link between the distribution of clusters size and an overall energy potential that translates the competition between aggregation and disaggregation processes. An increase in the adhesion induces a shift toward higher cluster sizes, and the algebraic dependence of the power-law exponent with the cluster fractal dimension predicted by our approach is the salient prediction of our model. We have also proposed a link between this exponent and the homogeneity coefficients of the (dis)-aggregation kernels in classical population balance models. Still, one should remain careful about a direct inference of one simple general formula as provided here, since many additional parameters may be involved in the size selection, including time through aging phenomena, spatial confinement, and individual cluster dynamics.

---

[1] C. W. Macosko, *Rheology: Principles, Measurements and Applications*, edited by C. W. Macosko (John Wiley & Sons, New York, NY, 1994).

[2] J. Mewis and N. J. Wagner, *Colloidal Suspension Rheology*, edited by J. Mewis and N. J. Wagner (Cambridge Univesity Press, Cambridge, UK, 2012).

[3] N. J. Wagner and J. Mewis, *Theory and Applications of Colloidal Suspension Rheology*, edited by N. J. Wagner and J. Mewis (Cambridge University Press, Cambridge, UK, 2021).

[4] N. Hengl, Y. Jin, F. Pignon, S. Baup, R. Mollard, N. Gondrexon, A. Magnin, L. Michot, and E. Paineau, A new way to apply ultrasound in cross-flow ultrafiltration: Application to colloidal suspensions, Ultrason. Sonochem. **21**, 1018 (2014).

[5] K. Ioannidou, K. J. Krakowiak, M. Bauchy, C. G. Hoover, E. Masoero, S. Yip, F.-J. Ulm, P. Levitz, R. J.-M. Pellenq, and E. Del Gado, Mesoscale texture of cement hydrates, Proc. Nat. Acad. Sci. USA **113**, 2029 (2016).

[6] T. S. Awad, H. A. Moharram, O. E. Shaltout, and M. M. Youssef, Applications of ultrasound in analysis, processing and quality control of food: A review, Food Res. Int. **48**, 410 (2012).

[7] D. Knorr, M. Zenker, V. Heinz, and D.-U. Lee, Applications and potential of ultrasonics in food processing, Trends Food Sci. Technol. **15**, 261 (2004).

[8] J. Chandrapala, C. Oliver, S. Kentish, and M. Ashokkumar, Ultrasonics in food processing, Ultrason. Sonochem. **19**, 975 (2012).

[9] D. Bonn, M. M. Denn, L. Berthier, T. Divoux, and S. Manneville, Yield stress materials in soft condensed matter, Rev. Mod. Phys. **89**, 035005 (2017).

[10] N. D. Vassileva, D. van den Ende, F. Mugele, and J. Mellema, Capillary forces between spherical particles floating at a liquid-liquid interface, Langmuir **21**, 11190 (2005).

[11] R. Wessel and R. C. Ball, Fractal aggregates and gels in shear flow, Phys. Rev. A **46**, R3008 (1992).

[12] W.-H. Shih, W. Y. Shih, S.-I. Kim, J. Liu, and I. A. Aksay, Scaling behavior of the elastic properties of colloidal gels, Phys. Rev. A **42**, 4772 (1990).

[13] C. M. Sorensen, Light scattering by fractal aggregates: A review, Aerosol Sci. Technol. **35**, 648 (2001).

[14] M. Y. Lin, R. Klein, H. M. Lindsay, D. A. Weitz, R. C. Ball, and P. Meakin, The structure of fractal colloidal aggregates of finite extent, J. Colloid Interface Sci. **137**, 263 (1990).

[15] S. Lazzari, L. Nicoud, B. Jaquet, M. Lattuada, and M. Morbidelli, Fractal-like structures in colloid science, Adv. Colloid Interface Sci. **235**, 1 (2016).

[16] P. Grassberger, On the spreading of two-dimensional percolation, J. Phys. A: Math. Gen. **18**, L215 (1985).

[17] M. Bantawa, W. A. Fontaine-Seiler, P. D. Olmsted, and E. Del Gado, Microscopic interactions and emerging elasticity in model soft particulate gels, J. Phys.: Condens. Matter **33**, 414001 (2021).

[18] D. A. Weitz and M. Oliveria, Fractal structures formed by kinetic aggregation of aqueous gold colloids, Phys. Rev. Lett. **52**, 1433 (1984).

[19] D. A. Weitz, J. S. Huang, M. Y. Lin, and J. Sung, Limits of the fractal dimension for irreversible kinetic aggregation of gold colloids, Phys. Rev. Lett. **54**, 1416 (1985).

[20] H. Hoekstra, J. Vermant, J. Mewis, and G. Fuller, Flow-induced anisotropy and reversible aggregation in two-dimensional suspensions, Langmuir **19**, 9134 (2003).

[21] V. S. Nguyen, D. Rouxel, R. Hadji, B. Vincent, and Y. Fort, Effect of ultrasonication and dispersion stability on the cluster size of alumina nanoscale particles in aqueous solutions, Ultrason. Sonochem. **18**, 382 (2011).

[22] J. J. Richards, J. B. Hipp, J. K. Riley, N. J. Wagner, and P. D. Butler, Clustering and percolation in suspensions of carbon black, Langmuir **33**, 12260 (2017).

[23] K. Masschaele, J. Fransaer, and J. Vermant, Direct visualization of yielding in model two-dimensional colloidal gels subjected to shear flow, J. Rheol. **53**, 1437 (2009).

[24] H. Hoekstra, J. Mewis, T. Narayanan, and J. Vermant, Multi length scale analysis of the microstructure in sticky sphere dispersions during shear flow, Langmuir **21**, 11017 (2005).

[25] A. Zaccone, M. Soos, M. Lattuada, H. Wu, M. U. Bäbler, and M. Morbidelli, Breakup of dense colloidal aggregates under hydrodynamic stresses, Phys. Rev. E **79**, 061401 (2009).

[26] F. E. Torres, W. B. Russel, and W. R. Schowalter, Floc structure and growth kinetics for rapid shear coagulationof polystyrene colloids, J. Colloid Interface Sci. **142**, 554 (1991).

[27] R. J. Hunter and J. Frayne, Flow behavior of coagulated colloidal sols, J. Colloid Interface Sci. **76**, 107 (1980).

[28] K. Higashitani and K. Iimura, Two-dimensional simulation of the breakup process of aggregates in shear and elongational flows, J. Colloid Interface Sci. **204**, 320 (1998).

[29] K. Higashitani, K. Iimura, and H. Sanda, Simulation of deformation and breakupof large aggregates in flows of viscous Fluids, Chem. Eng. Sci. **56**, 2927 (2001).

[30] R. Massaro, G. Colombo, P. Van Puyvelde, and J. Vermant, Viscoelastic cluster densification in sheared colloidal gels, Soft Matter **16**, 2437 (2020).

[31] J. F. Brady and G. Bossis, The rheology of concentrated suspensions of spheres in simple shear flow by numerical simulation, J. Fluid Mech. **155**, 105 (1985).

[32] J. F. Morris, A review of microstructure in concentrated suspensions and its implications for rheology and bulk flow, Rheol. Acta **48**, 909 (2009).

[33] Z. Varga, G. Wang, and J. Swan, The hydrodynamics of colloidal gelation, Soft Matter **11**, 9009 (2015).

[34] Z. Varga and J. W. Swan, Linear viscoelasticity of attractive colloidal dispersions, J. Rheol. **59**, 1271 (2015).

[35] Z. Varga and J. W. Swan, Large scale anisotropies in sheared colloidal gels, J. Rheol. **62**, 405 (2018).

[36] Z. Varga, V. Grenard, S. Pecorario, N. Taberlet, V. Dolique, S. Manneville, T. Divoux, G. H. McKinley, and J. W. Swan, Hydrodynamics control shear-induced pattern formation in attractive suspensions, Proc. Natl. Acad. Sci. USA **116**, 12193 (2019).

[37] T. Lorenzo and L. Marco, Brownian dynamics simulations of shear-induced aggregation of charged colloidal particles in the presence of hydrodynamic interactions, J. Colloid Interface Sci. **624**, 637 (2022).

[38] S. Jungblut, J.-O. Joswig, and A. Eychmüller, Diffusion- and reaction-limited cluster aggregation revisited, Phys. Chem. Chem. Phys. **21**, 5723 (2019).

[39] J. Colombo and E. Del Gado, Stress localization, stiffening, and yielding in a model colloidal gel, J. Rheol. **58**, 1089 (2014).

[40] M. Bouzid, B. Keshavarz, M. Geri, T. Divoux, E. Del Gado, and G. H. McKinley, Computing the linear viscoelastic properties of soft gels using an optimally windowed chirp protocol, J. Rheol. **62**, 1037 (2018).

[41] A. Kimbonguila Manounou and S. Rémond, Discrete element modeling of the microstructure of fine particle agglomerates in sheared dilute suspension, Physica A **412**, 66 (2014).

[42] M. L. Eggersdorfer, D. Kadau, H. J. Herrmann, and S. E. Pratsinis, Fragmentation and restructuring of soft-agglomerates under shear, J. Colloid Interface Sci. **342**, 261 (2010).

[43] X. Ruan, S. Chen, and S. Li, Structural evolution and breakage of dense agglomerates in shear flowand Taylor-Green vortex, Chem. Eng. Sci. **211**, 115261 (2020).

[44] M. Soos, J. Sefcik, and M. Morbidelli, Investigation of aggregation, breakage and restructuring kinetics of colloidal dispersions in turbulent flows by population balance modeling and static light scattering, Chem. Eng. Sci. **61**, 2349 (2006).

[45] M. Soos, L. Wang, R. O. Fox, J. Sefcik, and M. Morbidelli, Population balance modeling of aggregation and breakage in turbulent taylor–couette flow, J. Colloid Interface Sci. **307**, 433 (2007).

[46] A. Puisto, X. Illa, M. Mohtaschemi, and M. J. Alava, Modeling the viscosity and aggregation of suspensions of highly anisotropic nanoparticles, Eur. Phys. J. E **35**, 6 (2012).

[47] M. Lattuada, A. Zaccone, H. Wu, and M. Morbidelli, Population-balance description of shear-induced clustering, gelation and suspension viscosity in sheared DLVO colloids, Soft Matter **12**, 5313 (2016).

[48] J. Banasiak, W. Lamb, and P. Laurençot, *Analytic Methods for Coagulation-Fragmentation Models, Volume I*, edited by J. Banasiak, W. Lamb, and P. Laurençot, Monographs and Research Notes in Mathematics, Vol. 1 (CRC Press, Boca Raton, FL, 2020).

[49] Y. Kantor and T. A. Witten, Mechanical stability of tenuous objects, J. Phys. Lett. **45**, 675 (1984).

[50] M. Mellema, J. H. J. van Opheusde, and T. van Vliet, Categorization of rheological scaling models for particlegels applied to casein gels, J. Rheol. **46**, 11 (2002).

[51] L. B. Brakalov, Connection between the orthokinetic coagulation capture efficiency of aggregates and their maximum size, Chem. Eng. Sci. **42**, 2373 (1987).

[52] F. E. Torres, W. B. Russel, and W. R. Schowalter, Simulation of coagulation in viscous flows, J. Colloid Interface Sci. **145**, 51 (1991).

[53] P. Snabre and P. Mills, I. rheology of weakly flocculated suspensions of rigid particles, J. Phys. III **6**, 1811 (1996).

[54] J. S. Marshall and S. Li, *Adhesive Particle Flow: A Discrete-Element Approach*, 1st ed., edited by J. S. Marshall and S. Li (Cambridge University Press, Cambridge, UK, 2014).

[55] R. von Mises, Mechanik der festen Körper im plastisch-deformablen Zustand, Nachr. Gesellsch. Wissensc. Göttingen **1**, 582 (1913).

[56] A. A. Griffith, VI. The phenomena of rupture and flow in solids, Phil. Trans. R. Soc. A **221**, 163 (1921).

[57] G. R. Irwin, Analysis of stresses and strains near the end of a crack traversing a plate, J. Appl. Mech. **24**, 361 (1957).

[58] C. Creton and M. Ciccotti, Fracture and adhesion of soft materials: A review, Rep. Prog. Phys. **79**, 046601 (2016).

[59] E. Buckingham, On physically similar systems; illustrations of the use of dimensional equations, Phys. Rev. **4**, 345 (1914).

[60] E. Buckingham, The principle of similitude, Nature (Lond.) **96**, 396 (1915).

[61] E. Buckingham, Model experiments and the forms of empirical equations, in *Transactions of the American Society of Mechanical Engineers*, Vol. 37, American Society of Mechanical Engineers (American Society of Mechanical Engineers, New York, NY, 1915), pp. 263–296.

[62] S. Jamali, R. C. Armstrong, and G. H. McKinley, Time-rate-transformation framework for targeted assembly of short-range attractive colloidal suspensions, Mater. Today Adv. **5**, 100026 (2020).

[63] M. Nabizadeh and S. Jamali, Life and death of colloidal bonds control the rate-dependent rheology of gels, Nat. Commun. **12**, 4274 (2021).

[64] A. P. Thompson, H. M. Aktulga, R. Berger, D. S. Bolintineanu, W. M. Brown, P. S. Crozier, P. J. in 't Veld, A. Kohlmeyer, S. G. Moore, T. D. Nguyen, R. Shan, M. J. Stevens, J. Tranchida, C. Trott, and S. J. Plimpton, LAMMPS - a flexible simulation tool for particle-based materials modeling at the atomic, meso, and continuum scales, Comput. Phys. Commun. **271**, 108171 (2022).

[65] A. Stukowski, Visualization and analysis of atomistic simulation data with OVITO—The Open Visualization Tool, Modell. Simul. Mater. Sci. Eng. **18**, 015012 (2010).

[66] Additional simulations were carried out with various values of *C* and the main results remained similar up to a rescaling of the timescale.

[67] W. C. Swope, H. C. Andersen, P. H. Berens, and K. R. Wilson, A computer simulation method for the calculation of equilibrium constants for the formation of physical clusters of molecules: Application to small waterclusters, J. Chem. Phys. **76**, 637 (1982).

[68] D. J. Pearce, An Improved Algorithm for Finding the Strongly Connected Components of a Directed Graph (Victoria University, 2005), https://citeseerx.ist.psu.edu/viewdoc/summary?doi=10.1.1.102.1707.

[69] J. Colombo, A. Widmer-Cooper, and E. Del Gado, Microscopic Picture of Cooperative Processes in Restructuring Gel Networks, Phys. Rev. Lett. 110, 198301 (2013).

[70] J. Colombo and E. Del Gado, Self-assembly and cooperative dynamics of a model colloidal gel network, Soft Matter 10, 4003 (2014).

[71] J. Banasiak, W. Lamb, and P. Laurençot, *Analytic Methods for Coagulation-Fragmentation Models, Volume II*, edited by J. Banasiak, W. Lamb, and P. Laurençot, Monographs and Research Notes in Mathematics, Vol. 2 (CRC Press, Boca Raton, FL, 2020).

[72] F. Golse, The Boltzmann equation and its hydrodynamic limits, in *Handbook of Differential Equations: Evolutionary Equations* (Elsevier-North-Holland, Amsterdam, 2005), pp. 159–301.

[73] B. V. Alexeev, *Generalized Boltzmann Physical Kinetics*, edited by B. V. Alexeev (Elsevier, Amsterdam, 2004).

[74] V. Stadnichuk, A. Bodrova, and N. Brilliantov, Smoluchowski aggregation fragmentation equations: Fast numerical method to find steady-state solutions, Int. J. Mod. Phys. B 29, 1550208 (2015).

[75] Taking some usual examples leads to $\delta \approx \arg\min_{d \in \mathbb{R}_+^*} w(d)$.

[76] C. M. Sorensen, H. X. Zhang, and T. W. Taylor, Cluster-Size Evolution in a Coagulation-Fragmentation System, Phys. Rev. Lett. 59, 363 (1987).

[77] The homogeneity coefficients are defined as $K(\xi x, \xi y) = \xi^\lambda K(x, y)$ and $F(\xi x, \xi y) = \xi^\alpha F(x, y)$ for all $(x, y, \xi) \in \mathbb{R}_+^3$.

[78] J. A. D. Wattis, An introduction to mathematical models of coagulation–fragmentation processes: A discrete deterministic mean-field approach, Physica D 222, 1 (2006).

[79] P. T. Spicer and S. E. Pratsinis, Coagulation and fragmentation: Universal steady-state particle-size distribution, AIChE J. 42, 1612 (1996).

[80] I. Kryven, S. Lazzari, and G. Storti, Population balance modeling of aggregation and coalescence in colloidal systems, Macromol. Theory Simul. 23, 170 (2014).

[81] G. Barthelmes, S. E. Pratsinis, and H. Buggisch, Particle size distributions and viscosity of suspensions undergoing shear-induced coagulation and fragmentation, Chem. Eng. Sci. 58, 2893 (2003).

[82] M. A. Delichatsios and R. F. Probstein, The effect of coalescence on the average drop size in liquid-liquid dispersions, Ind. Eng. Chem. Fundam. 15, 134 (1976).

[83] K. A. Kusters, The Influence of Turbulence on Aggregation of Small Particles in Agitated Vessels, Ph.D. thesis (1991).

[84] R. C. Sonntag and W. B. Russel, Structure and breakup of flocs subjected to fluid stresses: I. Shear experiments, J. Colloid Interface Sci. 113, 399 (1986).

[85] R. C. Sonntag and W. B. Russel, Structure and breakup of flocs subjected to fluid stresses: II. Theory, J. Colloid Interface Sci. 115, 378 (1987).

[86] R. C. Sonntag and W. B. Russel, Structure and breakup of flocs subjected to fluid stresses: III. Converging flow, J. Colloid Interface Sci. 115, 390 (1987).

[87] Y. M. Harshe, M. Lattuada, and M. Soos, Experimental and modeling study of breakage and restructuring of open and dense colloidal aggregates, Langmuir 27, 5739 (2011).

[88] A. A. Potanin, On the mechanism of aggregation in the shear flow of suspensions, J. Colloid Interface Sci. 145, 140 (1991).

[89] A. A. Potanin, On the model of colloid aggregates and aggregating colloids, J. Chem. Phys. 96, 9191 (1992).

[90] A. A. Potanin and W. B. Russel, Fractal model of consolidation of weakly aggregated colloidal dispersions, Phys. Rev. E 53, 3702 (1996).

[91] T. Gibaud, N. Dagès, P. Lidon, G. Jung, L. C. Ahouré, M. Sztucki, A. Poulesquen, N. Hengl, F. Pignon, and S. Manneville, Rheoacoustic Gels: Tuning mechanical and Flow Properties of Colloidal Gels with Ultrasonic Vibrations, Phys. Rev. X 10, 011028 (2020).

[92] T. Gibaud, T. Divoux, and S. Manneville, Nonlinear mechanics of colloidal gels: Creep, fatigue and shear-induced yielding, in *Encyclopedia of Complexity and Systems Science* (Springer, Berlin, 2020), pp. 1–24.

[93] N. Dagés, P. Lidon, G. Jung, F. Pignon, S. Manneville, and T. Gibaud, Mechanics and structure of carbon black gels under high-power ultrasound, J. Rheol. **65**, 477 (2021).

[94] G. L. Klimchitskaya, U. Mohideen, and V. M. Mostepanenko, Casimir and van der waals force between two plates or a sphere (lens) above a plate made of real metals, Phys. Rev. A **61**, 062107 (2000).

[95] J. Visser, On Hamaker constants: A comparison between Hamaker constants and Lifshitz-Van der Waals constants, Adv. Colloid Interface Sci. **3**, 331 (1972).

[96] T. D. Waite, J. K. Cleaver, and J. K. Beattie, Aggregation kinetics and fractal structure of γ-alumina assemblages, J. Colloid Interface Sci. **241**, 333 (2001).